Supporting Information

Laine et al. 10.1073/pnas.0914611107

SI Text

SI Materials and Methods. ***Structure analysis.*** Four crystallographic structures of adenylyl cyclase (EF) were used in the present work: three structures of the EF-CaM complex [Protein Data Bank (PDB) ID codes: 1K93, 1K90, and 1XFX] and one of the free form of EF (PDB ID code: 1K8T) (1, 2). The crystallographic structure of CyaA catalytic domain in association with the C-terminal part of CaM (3) was also analyzed (PDB ID code: 1YRT).

Molecular dynamics simulations. Molecular dynamics (MD) simulations were performed using the modules sander and PMEMD of AMBER 8 and 10 (4). The MD simulations of the complex EF-CaM loaded with 0, 2, and 4 ions Ca^{2+} were as described previously (5). In addition, 15 ns MD simulation of the free EF in a closed conformation was performed in the same conditions, except that the temperature was regulated using a Langevin thermostat (6) with a collision frequency of 2 ps^{-1}.

In silico screening and analysis. Pockets were identified at the surface of analyzed proteins using the PocketFinder module (7) of the ICM software package (8). Histidine protonation for the receptor was assigned according to WHATIF (9) predictions. Mg^{2+} and Yb^{3+} ions were discarded for docking to the catalytic site.

2D structures of 30,976 compounds were downloaded from the French National Chemical Library (10) in Structure Data File format. Building of 3D structures, addition of hydrogens, and conversion to MOL2 format were performed using CORINA (11, 12). 2,647 compounds were removed because of building failure or presence of multiple fragments. ATP structure was downloaded from the "Biochemical Compounds Declarative Database" (13) and the 3D structures of 3'-deoxy-ATP were taken from the X-Ray crystallographic structures 1K90 (1) and 1XFX (2).

The docking was performed with FlexX (14), which proceeds through incremental construction of the ligand in the targeted binding site, aiming at maximizing protein–ligand interactions (15). FlexX standard scoring function, similar to the Böhm function (16), was used with default parameters. The ICM docking program (8, 17) was used to further score FlexX candidates with a thoroughness factor of 10, and 5 independent Monte Carlo runs for each compound.

The construction, clustering and visualization of structural interaction fingerprints (SIFt) (18–20) were performed with the R software (21). The similarity between SIFts was evaluated from their Tanimoto coefficient (22) and they were clustered through an agglomerative hierarchical clustering approach (23).

Synthesis of identified inhibitors. The identified inhibitors were issued from the chemical library of the CERMN (Centre d'Etudes et de Recherche sur le Médicament de Normandie). The CERMN developed a program of parallel synthesis (24, 25) to produce new thiophen derivatives with potential pharmacological properties. Thus, a library of 1,140 thiophen ureidoacids (TUA) was synthesized (Fig. S9) by the reaction of a set of 60 primary or secondary amines with a number of 19 thieno [3,2-d]- or thieno [2,3-d][1,3] oxazine-2,4-diones. The compounds were obtained by a simple solution-phase combinatorial strategy on a 200–400-mg scale. The yields were over 70% yields and the purities over 80%.

The synthesis of anhydrides [Fig. S9: **(3)**] started from the corresponding aminoesters [Fig. S9: **(1)**] prepared following a Kirsch method for 4-substituted aminoesters (26, 27) or an Arnold–Vilsmeier–Haack (28, 29) method for the 5-substituted aminoesters. The alkaline hydrolysis of these aminoesters under microwave heating conditions led to nonisolated aminocarboxylate intermediates **(2)**, and further addition of phosgene allowed to isolate anhydrides in high yields (73–82%). The anhydrides reacted in a water suspension with 2.2 equivalent of a primary or secondary amine and led to the water-soluble ammonium ureidothiophen [Fig. S9: **(4)**] carboxylates. An acidification of the reaction mixture allowed to recover the thienoureidoacid [Fig. S9: **(5)**] as a precipitated solid after filtration. A straightforward washing with water discarded excess of amine as a water-soluble hydrochloride.

Biochemical assay of compounds. Compounds were dissolved in DMSO to a 10 mM stock concentration and kept frozen at −20 °C until use. The proteins, EF, CyaA, and calmodulin (CaM) were purified as previously described (30–32). *Escherichia coli* inorganic pyrophosphatase (PPiase) was purchased from Sigma (ref I5907) and the Pi-ALS kit from Innova Biosciences (Innova Biosciences Ltd.).

Adenylate cyclase enzymatic assay. To characterize the inhibitory potential of the different compounds toward the bacterial adenylate cyclase (AC) toxins, a colorimetric assay for adenylyl cyclase activity in microplate format was designed. AC converts ATP into cAMP and inorganic pyrophosphate (PPi) that can be further cleaved by pyrophosphatase (PPiase, e.g., from *E. coli*, ref Sigma I5907) into two phosphate (Pi) molecules. These latter can be detected by colorimetry as an absorption change (read at 595 nm) of the malachite green dye in the presence of phosphomolybdate complexes.

Assays were carried out as follows. *Bacillus anthracis* EF was diluted into the AC assay buffer (20 mM Hepes-Na, pH 7.5, 15 mM $MgCl_2$, 0.2 mM $CaCl_2$, 0.01% Tween 20 (vol/vol) supplemented with 4 units/mL of PPiase (1 unit of PPiase hydrolyzes 1 μmol of PPi per minute) to a final concentration of 0.2–0.5 nM and 25 μL were distributed in the wells of a 96-well microplate. Compounds (10 μL from a 5× concentrated solutions in assay buffer) were added to the indicated final concentrations (i.e., 100, 10, or 1 μM) and incubated for 20 min at 22 °C. Then calmodulin (CaM, 5 μL from a 20 μM stock solution in assay buffer) was added to a final concentration of 2 μM and the mixtures were further incubated for 10 min at 30 °C. The enzymatic reaction was initiated by addition of ATP (10 μL, 2 mM final concentration) and the microplate was incubated at 30 °C under agitation. Ten-μL samples from each well were then taken out at different incubation times (from 3 to 15 min) and transferred into a second microtiter plate containing, in each well, 100 μL of a Pi-ALS mixture made of 10 μL of H_2O, 80 μL of Pi ColorLock ALS reagent and 10 μL Accelerator solution (both provided in the Pi-ALS kit from Innova Biosciences): The enzymatic reaction was immediately stopped by the acidic conditions of this Pi-ALS mixture. After 5 min of incubation at room temperature, 10 μL of stabilizer solution (from the Pi-ALS kit) were added to prevent further nonenzymatic breakdown of the phosphorylated substrate under acidic conditions (according to the kit instructions). After a further 30–60 min of incubation at room temperature, the Optical Densities at 595 nm (OD_{595}) were recorded with a microplate reader (Tecan).

A standard curve was performed in parallel by adding known concentrations of Pi into Pi-ALS mixture and used to convert OD_{595} values into moles of produced PPi. The enzymatic activity

was calculated from the initial velocity of PPi synthesis (in the above described conditions, accumulation of PPi was linear with time and PPiase was in about 100 times excess). In the absence of compounds, the specific activity of EF was found to be between 1 and 2 mmol PPi per min and mg of protein (corresponding to 100% activity). When CaM was omitted in the assay mixture, the PPi synthesis activity was below the detection level (i.e., <1 μmol PPi per min and mg of protein, corresponding to 0% activity). In some experiments (see *Results*), CaM was mixed with EF **prior** to the addition of the compounds.

Bordetella pertussis CyaA was assayed similarly at a final concentration of 0.1–0.2 nM. CyaA specific activity was 2.5 mmol PPi per min and mg of protein in the presence of CaM and below the detection level (i.e., <1 μmol PPi per min and mg of protein) in the absence of CaM.

CaM-binding properties probed by steady-state fluorescence anisotropy. A N-acetylated peptide, $P_{233-254}$, corresponding to main CaM-binding sequence of CyaA (33) Ac-LDRERIDLLWKIARAGARSAVG was synthesized by Genosphere Biotechnologies. Calcium-dependent binding of $P_{233-254}$ to CaM was measured by steady-state fluorescence anisotropy of its unique tryptophan (CaM has no tryptophan) in a FP-6200 spectrofluorimeter (Jasco) and a Peltier-thermostated cell holder at 25 °C, using a 1 cm path length quartz cell (101.QS from Hellma). The excitation wavelength was 295 nm and emission spectra were recorded from 300 to 400 nm. Bandwidths were 5 and 10 nm for excitation and emission, respectively. Tryptophan anisotropy of $P_{233-254}$ (2 μM) was measured with or without CaM (2 μM) and/or TUA-diCl (10 μM) in buffer A (20 mM Hepes, 150 mM NaCl, pH 7.4) supplemented with 0.2 mM $CaCl_2$ or 2 mM EGTA. Steady-state fluorescence anisotropy experiments were performed with vertically (V) and horizontally (H) polarized beam light using FDP-223 polarizers at both excitation (x) and emission (m) apertures. Anisotropy values (r), measured at a wavelength of 345 ± 1 nm, were calculated as follows:

$$r = \frac{V_x V_m - \frac{H_x V_m}{H_x H_m} V_x H_m}{V_x V_m + 2\frac{H_x V_m}{H_x H_m} V_x H_m}. \qquad \textbf{[S1]}$$

1. Drum C, et al. (2002) Structural basis for the activation of Anthrax adenylyl cyclase exotoxin by calmodulin. *Nature* 415:396–402.
2. Shen Y, Zhukovskaya N, Guo Q, Florin J, Tang W (2005) Calcium-independent calmodulin binding and two-metal-ion catalytic mechanism of Anthrax edema factor. *EMBO J* 24:929–941.
3. Guo Q, et al. (2005) Structural basis for the interaction of Bordetella pertussis adenylyl cyclase toxin with calmodulin. *EMBO J* 24:3190–3201.
4. Case D, et al. (2004) AMBER 9. University of California.
5. Laine E, Yoneda J, Blondel A, Malliavin T (2008) The conformational plasticity of calmodulin upon calcium complexation gives a model of its interaction with the oedema factor of Bacillus anthracis. *Proteins* 71:1813–1829.
6. Loncharich R, Brooks B, Pastor R (1992) Langevin dynamics of peptides: The frictional dependence of isomerization rates of N-acetylalanyl-N′-methylamide. *Biopolymers* 32:523–535.
7. An J, Totrov M, Abagyan R (2004) Comprehensive identification of druggable protein ligand binding sites. *Genome Inform* 15:31–41.
8. Abagyan R (2005) *ICM Manual v.3.1* (Molsoft LLC, La Jolla, CA).
9. Vriend G (1990) WHAT IF: A molecular modeling and drug design program. *J Mol Graph* 8:52–56.
10. (2008), Chimiothèque nationale du cnrs, http://chimiotheque-nationale.enscm.fr.
11. Sadowski J, Gasteiger J, Klebe G (1994) Comparison of automatic three-dimensional model builders using 639 x-ray structures. *J Chem Inf Comp Sci* 34:1000–1008.
12. Sadowski J, Gasteiger J (1993) From atoms and bonds to three-dimensional atomic coordinates: Automatic model builders. *Chem Rev* 93:2567:2581.
13. (2008) ATP structure, http://www.biocheminfo.org/klotho/.
14. Rarey M (2007) FlexX release 2.1 User Guide, Technical report, BioSolveIt.
15. Rarey M, Kramer B, Lengauer T, Klebe G (1996) A fast flexible docking method using an incremental construction algorithm. *J Mol Biol* 261:470–489.
16. Böhm H (1994) The development of a simple empirical scoring function to estimate the binding constant for a protein-ligand complex of known three-dimensional structure. *J Comput Aided Mol Des* 8:243–256.
17. Totrov M, Abagyan R (1997) Flexible protein-ligand docking by global energy optimization in internal coordinates. *Proteins* Suppl 1:215–220.
18. Deng Z, Chuaqui C, Singh J (2004) Structural interaction fingerprint (SIFt): A novel method for analyzing three-dimensional protein-ligand binding interactions. *J Med Chem* 47:337–344.
19. Marcou G, Rognan D (2007) Optimizing fragment and scaffold docking by use of molecular interaction fingerprints. *J Chem Inf Model* 47:195–207.
20. Brewerton S (2008) The use of protein-ligand interaction fingerprints in docking. *Curr Opin Drug Discov Devel* 11:356–364.
21. Ihaka R, Gentleman R (1996) R: A language for data analysis and graphics. *J Comp Graph Statist* 5:299–314.
22. Willett P, Barnard J, Downs G (1998) Chemical similarity searching. *J Chem Inf Comput Sci* 38:983–996.
23. Hartigan J (1975) *Clustering Algorithms* (Wiley, New York).
24. LeFoulon F, Braud E, Fabis F, Lancelot JC, Rault S (2003) Synthesis and combinatorial approach of the reactivity of 6-and 7-arylthieno[3,2-d][1,3]oxazine-2,4-diones. *Tetrahedron* 59:10051–10057.
25. LeFoulon FX, Braud E, Fabis F, Lancelot JC, Rault S (2005) Solution-phase parallel synthesis of a 1140-member ureidothiophene carboxylic acid library. *J Comb Chem* 7:253–257.
26. Kirsch G, Caignant D, Caignant P (1982) Synthesis of 3-aminothiophenes from aryl-and hetarylacetonitriles. *J Heterocycl Chem* 19:443–445.
27. Rault S, Lancelot J, Letois B, Robba M, Labat Y (1995) Preparation of 3-mercapto-2-thiophenecarboxylic acid derivatives as intermediates for herbicides. French Patent No 9203732 *Chem Abstr* 123:11841.
28. Liebscher J, Neumann B, Hartmann H (1983) Eine einfache Synthese von-Chlorzimtsüreenitrilen nach einer modifizierten Vilsmeier-Haack-Arnold-Reaktion. *J Prakt Chem* 325:915–918.
29. Hartmann H, Liebscher J (1984) A simple method for the synthesis of 5-Aryl-3-amino-2-alkoxycarbonylthiophenes. *Synthesis* pp. 275–276.
30. Shen Y, et al. (2002) Physiological calcium concentrations regulate calmodulin binding and catalysis of adenylyl cyclase exotoxins. *EMBO J* 21:6721–6732.
31. Vougier S, et al. (2004) Essential role of methionine residues in calmodulin binding to Bordetella pertussis adenylate cyclase, as probed by selective oxidation and repair by the peptide methionine sulfoxide reductases. *J Biol Chem* 279:30210–30218.
32. Karimova G, et al. (1998) Charge-dependent translocation of Bordetella pertussis adenylate cyclase toxin into eukaryotic cells: Implication for the in vivo delivery of CD8+ T-cell epitopes into antigen-presenting cells. *Proc Natl Acad Sci USA* 95:12532–12537.
33. Ladant D, et al. (1989) Characterization of the calmodulin-binding and of the catalytic domain of Bordetella pertussis adenylate cyclase. *J Biol Chem* 264:4015–4020.
34. McDonald I, Thornton J (1994) Satisfying hydrogen bonding potential in proteins. *J Mol Biol* 238:777–793.
35. Wallace A, Laskowski R, Thornton J (1995) LIGPLOT: A program to generate schematic diagrams of protein-ligand interactions. *Prot Eng* 8:127–134.
36. Lyman E, Zuckerman D (2006) Ensemble-based convergence analysis of biomolecular trajectories. *Biophys J* 91:164–172.
37. Deng Z, Chuaqui C, Singh J (2004) Structural interaction fingerprint (SIFt): A novel method for analyzing three-dimensional protein-ligand binding interactions. *J Med Chem* 47:337–344.

Table S1. Pockets identified near SABC location at the surface of representative conformations (36) extracted at 1,012, 3,652, 7,348, 8,201, 12,078, and 14,401 ps from the 15-ns MD trajectory of closed EF

Conformation (ps)	Pocket number	Volume (Å^3)	Residues in common with SABC
1,012	p1	545	(3/23 = 13%) A496, Y626, N629
(15/16)	p2	323	(0/9 = 0%)
	p3	256	(7/13 = 54%) E539, P542, S544, Q553, Q581, Y627, N629
	p6	177	(11/14 = 79%) A496, P499, I538, E539, W552, Q553, T579, Q581, L625, Y627, N709
3,652	p1	1,170	(4/33 = 12%) P542, S544, Q553, Y627
(10/16)	p2	667	(3/25 = 12%) Q553, Y627, N629
	p5	188	(8/13 = 62%) P499, I538, E539, Q553, Q581, L625, Y627, N709
7,348	p1	391	(4/25 = 16%) A496, Q581, Y627, N629
(12/16)	p2	491	(11/21 = 52%) P499, E539, P542, W552, Q553, T579, Q581, L625, Y627, N629, N709
	p3	373	(0/16 = 0%)
8,201	p1	450	(0/26 = 0%)
(11/16)	p2	422	(11/17 = 65%) A496, P499, I538, P542, W552, Q553, T579, Q581, L625, Y627, N709
12,078	p1	735	(2/27 = 7%) Q581, N629
(10/16)	p2	817	(8/29 = 28%) P499, I538, P542, W552, Q553, L625, Y627, N709
14,401	p1	789	(0/26 = 0%)
(9/16)	p2	748	(9/28 = 32%) P499, I538, P542, W552, T579, Q581, L625, Y627, N709
	p3	175	(0/10 = 0%)
	p6	144	(0/10 = 0%)

For each pocket; its name given by ICM PocketFinder, its volume, the relative number, and the name of the residues in common with the SABC pocket are reported. Under each conformation number, the number of residues common to the ensemble of pockets and SABC is given in parentheses.

Table S2. Docking scores of the 1% best ligands of the 3,649 retained compounds onto the SABC pocket

Compound name	Conf1 (FlexX)	1K8T (FlexX)	Conf1 (ICM)	Conf1 (FlexX mean)	Conf8 (FlexX)	Conf28 (FlexX)	Conf47 (FlexX)
Not received	−37.71	−32.69	−22.36	−33.42 ± 1.95	−22.33	−15.66	−15.88
CEsr-1753000	−34.94	−30.45	−27.25	−32.41 ± 1.31	−19.88	−16.85	−13.95
Discarded •	−34.06	−32.63	[−2.59;−6.18]	−33.22 ± 0.31	−26.79	−24.13	−19.58
CEsr-1028000	−33.24	−30.20	[−11.86;−14.68]	−24.79 ± 2.95	−19.14	−12.84	−14.81
Not received	−33.12	−28.34	[−18.01;−24.83]	−31.25 ± 0.68	−24.75	−16.85	−14.70
Not received	−32.36	−32.51	[−12.54;−23.95]	−27.70 ± 2.15	−22.88	−15.94	−14.66
Discarded ⋆	−30.57	−34.93	−11.98	−26.32 ± 1.32	−26.88	−16.97	−19.84
Discarded ⋆	−30.04	−33.73	[−6.40;−14.15]	−24.99 ± 2.88	−26.29	−13.35	−16.21
CN014795V	−29.57	−25.52	−13.88	−25.69 ± 1.05	−14.00	−3.05	−3.96
Discarded •	−29.55	−32.08	+4.05	−28.21 ± 0.58	−23.16	−19.30	−12.56
CEsr-1759000	−29.44	−27.81	[−23.30;−26.14]	−26.20 ± 1.95	−18.81	−14.33	−16.10
Not received	−28.85	−29.13	[−15.17;−28.01]	−24.48 ± 1.17	−18.81	−12.46	−11.05
LPS_02-29-L-C07	−28.71	−30.21	[−18.05;−19.80]	−25.14 ± 1.25	−21.41	−13.52	−13.13
CEsr-1562400	−28.54	−28.06	[−19.82;−28.72]	−24.46 ± 1.37	−20.62	−12.77	−12.81
CEsr-5494000	−28.40	−32.60	[−19.17;−22.60]	−25.12 ± 1.03	−20.93	−17.75	−15.64
CEsr-3438000	−28.36	−23.52	[−11.88;−17.18]	−22.01 ± 2.52	−9.51	−3.58	−6.89
Discarded •	−28.31	−23.72	+5.49	−24.96 ± 1.12	−13.49	−12.28	−4.77
CEsr-4452000 ◇	−28.12	−30.74	[−20.60;−20.92]	−22.73 ± 2.51	−19.25	−12.62	−15.82
Not received	−27.93	−25.92	[−20.28;−21.45]	−24.82 ± 1.64	−17.47	−7.22	−10.51
CEsr-445600 ◇	−27.86	−30.74	[−19.39;−20.53]	−22.88 ± 2.29	−19.25	−12.24	−15.82
CEsr-5600000	−27.82	−33.33	[−18.52;−18.94]	−22.10 ± 1.59	−19.69	−13.84	−14.52
Not received	−27.67	−18.36	[−18.41;−18.63]	−18.97 ± 3.72	−16.42	−8.01	−7.81
CEsr-3341000 ◇	−27.66	−30.74	[−11.46;−23.53]	−22.94 ± 2.17	−19.25	−14.45	−15.82
CN013777V	−27.63	−28.79	[−17.77;−22.75]	−25.54 ± 0.71	−23.20	−14.55	−8.29
Not received	−27.62	−26.68	[−18.58;−18.82]	−23.66 ± 1.66	−16.28	−12.99	−12.17
CN013774V	−27.53	−27.51	[−21.66;−23.71]	−26.10 ± 0.45	−20.53	−14.17	−6.10
CEsr-4454000 ◇	−27.51	−30.74	[−19.00;−19.45]	−22.78 ± 2.25	−20.53	−13.28	−15.89
Not received	−27.33	−28.28	[−10.77;−11.01]	−22.33 ± 1.66	−17.00	−16.17	−12.20
CEsr-4451000 ◇	−27.31	−31.16	[−16.30;−18.89]	−23.89 ± 2.06	−19.38	−12.90	−16.05
Discarded •	−27.16	−19.26	[−8.09;−11.02]	−20.30 ± 2.61	−10.54	−6.72	−7.26
Not received	−27.16	−35.03	[−17.29;−27.46]	−25.70 ± 0.66	−24.21	−16.68	−19.41
Discarded ⋆ •	−27.14	−39.96	Cannot dock	−25.47 ± 0.89	−34.03	−2.71	−7.99
Not received	−27.12	−20.33	[−22.14;−24.48]	−20.27 ± 2.50	−6.07	−2.48	−5.36
CEsr-3342000 ◇	−27.09	−29.43	[−19.85;−20.68]	−24.62 ± 1.76	−17.85	−13.44	−14.76
Not received	−27.07	−35.36	[−16.03;−24.44]	−22.55 ± 1.34	−21.20	−13.42	−10.12
CEsr-1754000	−27.07	−21.44	[−10.75;−19.06]	−23.24 ± 1.50	−13.70	−10.21	−7.00

Best docking scores obtained with FlexX are given for the initial conformation *1* of the transition path, the crystallographic structure of closed EF 1K8T (1), and the intermediate conformations *8*, *28*, and *47* of the transition path. FlexX mean score for the conformation *1* is evaluated over the 20 best ranked docking poses of each compound. ICM score intervals reflect the range of best ICM scores obtained over 5 docking runs. • and ⋆ indicate compounds eliminated because of their bad ICM scores or their bad performance against the negative controls conformations *8*, *28*, and *47*, respectively. ◇ indicate selected compounds that were validated in vitro as inhibitors of EF activity.

Table S3. Residues from SABC pocket of EF and their corresponding residues in CyaA taken from the EF and CyaA sequences alignment (1)

EF		CyaA	
pre-SA	A496⋆	A193⋆	pre-F
pre-SA	P499⋆	P196⋆	pre-F
SA	I538	G254	helix H′
SA	E539	T255	helix H′
SA	P542	G265	β-hairpin between helices H′ and I
SA	S544	M267	β-hairpin between helices H′ and I
CA	S550 △	T273 △	CA
CA	W552 △	F275 △	CA
CA	Q553 ○	E276 ○	CA
SB	T579 ⋆	T300⋆	T300-K312 loop
SB	Q581 ⋆	Q302⋆	T300-K312 loop
SC	L625 △	V343 △	C-tail
SC	Y626 ○	F344 ○	C-tail
SC	Y627 ⋆	Y345⋆	C-tail
SC	N629 ⋆	N347	C-tail
Hel	N709		

⋆, identical residues; △, similar residues; and ○, residues sharing a common shape.

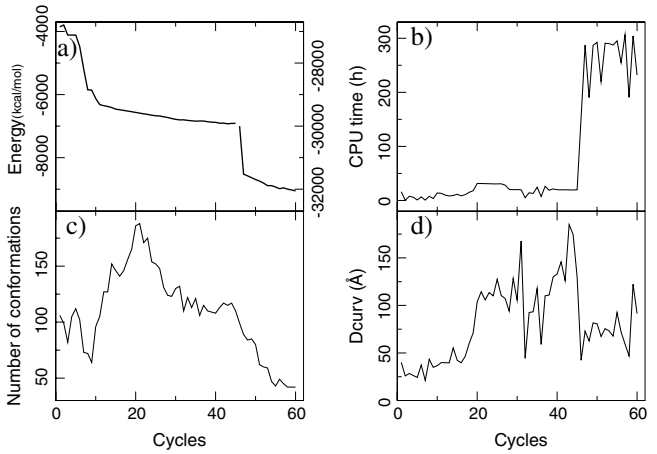

Fig. S1. Historic of the transition path refinement: (*a*) maximum energy, left and right scales for cycles calculated with sigmoidal or comprehensive electrostatics respectively; the line is broken to show the change in electrostatics, (*b*) refinement CPU time, (*c*) the number of conformations after the reduction and (*d*) path curvilinear length D_{curv} before reduction are given.

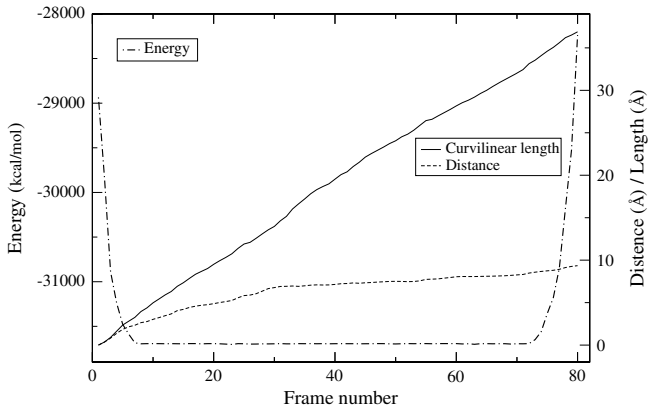

Fig. S2. Features of the final conformational transition path: energy, distance (coordinate rmsd) to the starting point of the path, curvilinear length D_{curv}, as a function of intermediate structure number in the path.

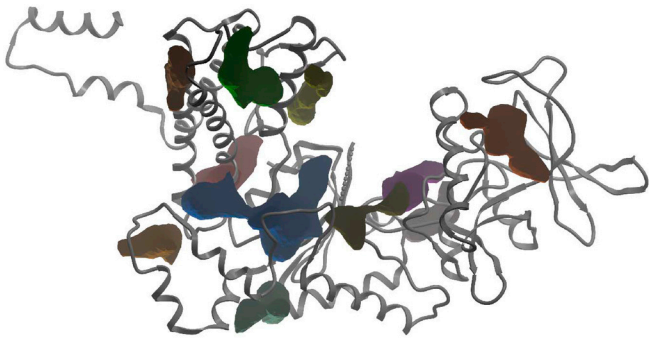

Fig. S3. Pockets detected at the surface of EF structure 1K8T (1) by ICM PocketFinder (7). The disordered loop (residues 580–590) of the structure is represented by a dashed line. A total of eleven pockets are identified with volumes ranging from 100 to 800 $Å^3$. Many pockets could be targeted, specifically close to the catalytic site.

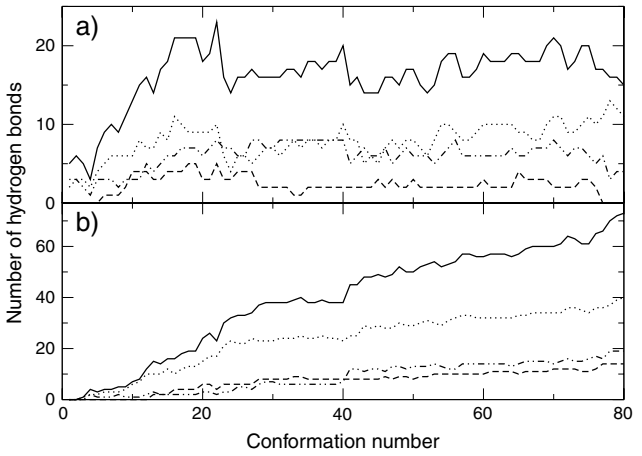

Fig. S4. Evolution of hydrogen bonds between switches A, B, and C during the transition. The numbers of hydrogen bonds between pairs of switches are plotted by dots-dashes, dashes, dots, and full lines for SA-SB, SA-SC, SB-SC, and the sum of the three pairs, respectively. (*a*) The number of hydrogen bonds for each conformation of the transition. (*b*) The number of hydrogen bonds ever formed from the first to the *n*th conformation that have been broken. Hydrogen bonds were identified with the HBPLUS 2.25 program (34) in the LIGPLOT 4.4.2 package (35). Switches A, B, and C were defined as residues 502–551, 578–591, and 623–659, respectively.

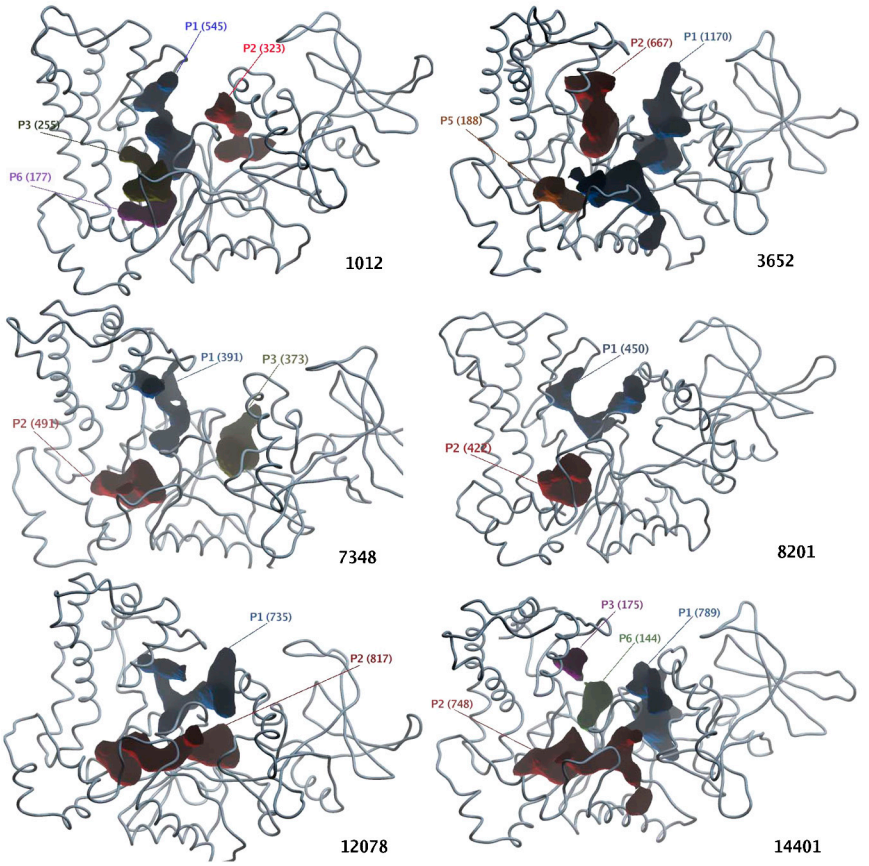

Fig. S5. Pockets identified on the representative conformations extracted from the MD simulations of isolated EF. It took 1 ns for the coordinate rmsd from the starting structure to stabilize around 3 Å. The backbone rmsd of switch B had a mean value of about 1.78 Å, with a standard deviation of 0.24 Å and a maximum value of 2.42 Å. Fluctuations do not exceed 2.2 Å for those residues and the secondary structure of the switch is almost completely stable after 5 ns. The position of each conformation into the simulation is indicated in the bottom right. The pockets are labeled P1 to P6, along with their volumes in $Å^3$.

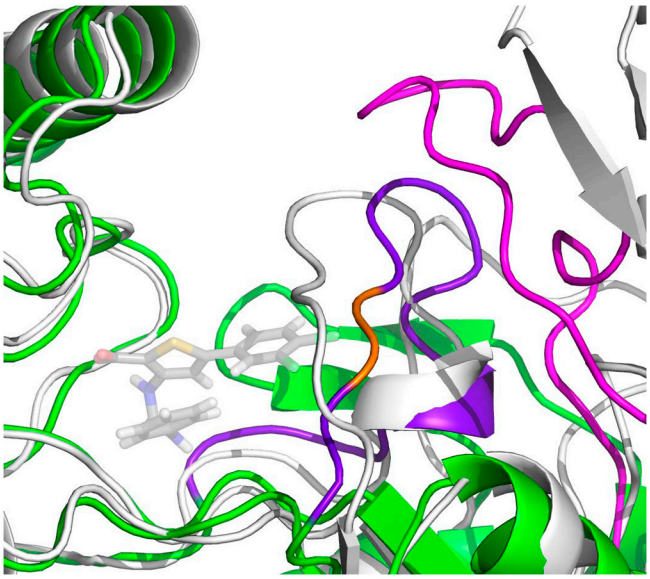

Fig. S6. Superimposition of inactive and active forms of the catalytic site. For the superimposition, the catalytic site is defined by residues R329, K346, L348, H351, K353, S354, K372, D491, D493, T548, H577, T579, D582, N583, F586, and E588 (1). Conformation *1* is displayed in white cartoons. Conformation *80* is displayed in colored cartoons: Switch C is in magenta, Switch B in purple, and the remaining regions are in green. The superimposition reveals moderate conformational change of the active site. To illustrate possible steric constraints, a model of TUAdiCl docked to the inactive form of the catalytic site (conformation *1*) was built with FlexX (14) and displayed with shadowed stick (carbons colored in white). The region of active conformation *80* (E588 and K589) that could clash with that TUAdiCl model is highlighted in orange. This region is in an extended conformation without strong interactions with the core of the protein. This shows that the conformational constraint imposed by the binding of an inhibitor to the inactive form of the catalytic site should have mainly local structural impact, and thus should not impede the binding of CaM on its remote binding site.

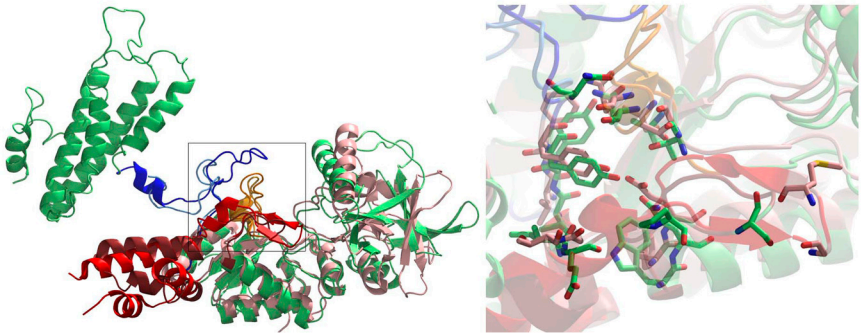

Fig. S7. Superimposition of EF (1K93, in lime) and CyaA (1YRT, in pink) structures, in complex with CaM. Switch A is highlighted in dark red and red, switch B in brown and orange, and switch C in blue and cyan, for EF and CyaA, respectively. A zoom of the SABC region (squared on the left) is represented on the right. The residues defining the pocket SABC are shown in sticks.

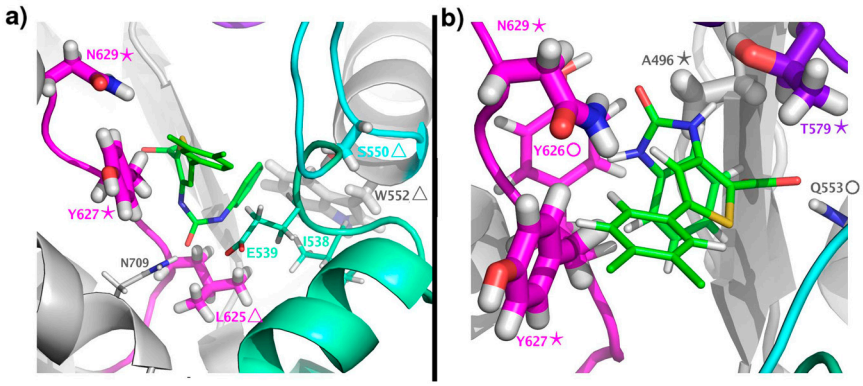

Fig. S8. TUAdiCl binding mode to the SABC pocket. TUAdiCl predicted docking poses were clustered through a structural interaction fingerprints (SIFt) analysis (19, 37). Poses grouped in the same cluster feature the same key interactions with the SABC binding pocket. Poses displayed are (*a*) the best pose, isolated in a singleton; (*b*) a representative pose from cluster 1, which contains poses 2–6, 9, and 13. TUAdiCl is displayed in licorice (carbons in green) together with the interacting residues of the SABC pocket. Switch A is colored in green-cyan, Switch B in indigo, Switch C in magenta, and the remaining residues in gray. The size of the licorice radii and the symbols added to the labels indicate the degree of similarity between the interacting residues and their counterparts in CyaA (see Table S3): ⋆ identical residues (very large radius), △ similar residues (large radius), and ○ residues sharing a common shape (medium radius).

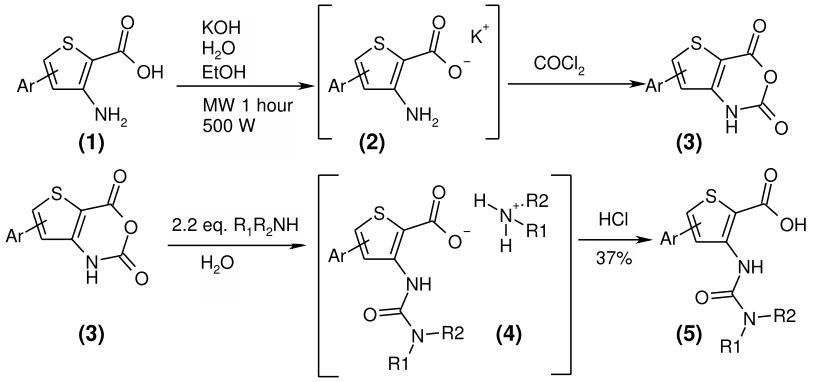

Fig. S9. Synthesis of a thiophen ureidoacids (TUA) library.